# Microtubules Contribute to the Birefringence of the Retinal Nerve Fiber Layer

*Xiang-Run Huang and Robert W. Knighton*

**Purpose.** The retinal nerve fiber layer (RNFL) exhibits birefringence that is due to the oriented cylindrical structure of the ganglion cell axons. Possible birefringent structures include axonal membranes, microtubules (MTs), and neurofilaments. MTs are generally assumed to be a major contributor, but this has not been demonstrated. In this study, the MT depolymerizing agent colchicine was used to evaluate the contribution of MTs to RNFL birefringence.

**Methods.** Retinal nerve fiber bundles of isolated rat retina were observed through an imaging polarimeter set near extinction. Images were taken over an extended period. During baseline, the tissue was perfused with a physiological solution. During a treatment period, the solution was switched either to a control solution identical with the baseline solution or to a similar solution containing colchicine. The contrast of nerve fiber bundles was used to follow change of RNFL birefringence over time.

**Results.** When imaged by the polarimeter, birefringent retinal nerve fiber bundles appeared as either bright or dark stripes. Bundles displayed as bright stripes were used to follow changes in retardance. The contrast of nerve fiber bundles was stable in control experiments. However, in treatment experiments, bundles were bright during the baseline period, but the contrast of bundles decreased rapidly when the colchicine solution was applied; bundles were barely visible after 30 minutes of treatment. After 70 minutes, the bundle contrast was close to zero at all wavelengths studied (440–780 nm).

**Conclusions.** MTs make a significant contribution to RNFL birefringence. The decrease of RNFL birefringence in glaucoma may indicate a loss of MTs. (*Invest Ophthalmol Vis Sci.* 2005; 46:4588–4593) DOI:10.1167/iovs.05-0532

The retinal nerve fiber layer (RNFL) in humans consists of bundles of unmyelinated ganglion cell axons running just under the surface of the retina.[1] The RNFL is damaged in glaucoma and other diseases of the optic nerve. To help diagnose and manage these diseases, various optical methods have been developed to assess the RNFL. One such method, scanning laser polarimetry (SLP), detects the birefringence of the peripapillary RNFL.[2,3] Clinical studies have found that changes in RNFL birefringence may correlate with damage in glaucoma.[4–6] Recent studies in measuring the birefringence distribution of the RNFL in human eyes strongly suggest that RNFL birefringence depends on axonal structure.[7,8] There exists, however, only limited knowledge of the mechanism responsible for RNFL birefringence.

Tissue birefringence includes two types: form birefringence, due to preferential orientation of cellular organelles, and intrinsic birefringence, due to anisotropic molecular structure.[9–11] An array of parallel cylindrical structures in a medium of different refractive index exhibits form birefringence.[12] Nerve fiber bundles contain oriented cylindrical organelles, including microtubules (MTs), neurofilaments, and axonal membranes,[13,14] and the RNFL is generally assumed to be form birefringent.

A theoretical model developed by Hemenger[15] shows that an array of thick cylinders with low relative refractive index can produce form birefringence that varies with wavelength. The birefringence of the RNFL, however, is constant across visible and near-infrared wavelengths,[16] a result that argues against a contribution by thick cylinders and suggests that the most likely mechanism for RNFL birefringence is form birefringence due to thin cylindrical structures. Theoretical calculations predict that axonal membranes should exhibit substantially higher form birefringence than MTs,[14] but the intrinsic birefringence of membranes may be sufficiently strong to cancel their form birefringence.[17] The birefringence of neurofilaments, which have one half the diameter of MTs, should be one fourth that of MTs for the same fibril density.[14] Currently, the commonly accepted hypothesis is that MTs are the primary source of RNFL birefringence.[2,7,8,16] This hypothesis is attractive, because MTs are the source of birefringence in other tissues—for example, mitotic spindles and crab axons[9,18,19]—but the role of MTs in RNFL birefringence has not been established by experiment.

Axonal MTs are long (10–25 $\mu$m), hollow cylinders with outer and inner diameters of approximately 25 and 15 nm, respectively.[20] MTs are polymers of tubulin, protein heterodimers that join end-to-end to maintain the structure of the MTs in a state of dynamic equilibrium. The antimitotic agent colchicine irreversibly binds to tubulin and leads to depolymerization of MTs.[21–23] Colchicine binding is specific to the subunit protein of microtubules,[22] and the morphology of tissues treated with colchicine does not appear to exhibit changes in the structural organization of axonal organelles other than a decrease in the number of MTs.[24] Thus, if MTs contribute to birefringence, colchicine treatment should cause the birefringence to decline. In this study, the role of MTs was determined by evaluating RNFL birefringence in isolated rat retina before and after treatment with colchicine.

## Methods and Materials

### Tissue Preparation and Perfusion Solutions

Rat retinas were chosen for the experiments for the following reasons: First, as in humans, the axons in the rat RNFL are not myelinated; second, nerve fiber bundles in rat retinas are separated by gaps, retinal regions without nerve fiber bundles, that allow correction for the polarization properties of the retina[16,25]; and finally, the birefringence property of rat retina has been well investigated.[16] The protocol for the use of animals was approved by the Animal Care and Use Committee

From the Bascom Palmer Eye Institute, University of Miami Miller School of Medicine, Miami, Florida.

Supported by National Institutes of Health Grant R01 EY008684, National Institutes of Health Core Grant P30-EY014801, and Research to Prevent Blindness.

Submitted for publication April 28, 2005; revised July 28, 2005; accepted October 10, 2005.

Disclosure: **X.-R. Huang**, None; **R.W. Knighton**, None

The publication costs of this article were defrayed in part by page charge payment. This article must therefore be marked "*advertisement*" in accordance with 18 U.S.C. §1734 solely to indicate this fact.

Corresponding author: Xiang-Run Huang, Bascom Palmer Eye Institute, University of Miami Miller School of Medicine, 1638 NW Tenth Avenue, Miami, FL 33136; xhuang3@med.miami.edu.

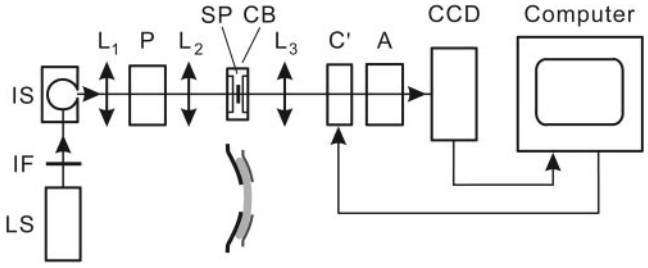


**FIGURE 1.** Schematic diagram of the multispectral imaging micropolarimeter used in transmission mode. LS, light source; IF, interference filter; IS, integrating sphere; P, linear polarizer; SP, specimen; CB, chamber; $L_1$, $L_2$, and $L_3$, lenses; C′, linear retarder; A, linear analyzer; CCD, charge-coupled device. *Inset*: diagram of the retina (*gray curve*) mounted between two membranes (*thick* and *thin black curves*) with slits.

of the University of Miami and procedures adhered to the ARVO Statement for the Use of Animals in Ophthalmic and Vision Research. Tissue was prepared according to previously developed procedures.[26] Briefly, the eye of an anesthetized rat was removed, and the animal was euthanatized. An eyecup of 5-mm diameter that included the optic nerve was excised and placed in a dish of warm (33–35°C) oxygenated physiologic solution. The retina was dissected from the retinal pigment epithelium and choroid with a fine glass probe and then draped across a slit in a black membrane with the photoreceptor side against the membrane. A second, thinner membrane with a slit matched to the black membrane was put on the RNFL surface to stretch the retina gently and eliminate wrinkles (Fig. 1, inset). The mounted retina was placed in a chamber perfused with warm physiologic solution to maintain the tissue alive.

An experiment consisted of a baseline period during which the chamber was perfused with a solution containing no colchicine, followed by a treatment period during which the solution was switched, either to a solution containing colchicine or a control solution identical with the baseline solution. Each period lasted approximately 1 hour. The perfusion fluids were based on a solution containing 110 mM NaCl, 5.0 mM KCl, 30 mM $NaHCO_3$, 0.8 mM $Na_2HPO_4$, 1.0 mM $MgCl_2$, 1.8 mM $CaCl_2$, 22 mM glucose, and 0.25 mM glutamine. The solutions were bubbled with a humidified gas mixture of 95% $O_2$ and 5% $CO_2$ (pH = 7.55–7.65). Because electron microscopy has shown that 10 mM colchicine significantly decreases the density of axonal MTs,[24,27] this concentration was added to the base solution to form the colchicine solution. To avoid retinal turbidity caused by osmotic change when switching to the colchicine solution,[27] an additional 10 mM glucose was added to the base solution to form the baseline and control solutions.

## Multispectral Imaging Micropolarimeter

RNFL birefringence causes light polarized along nerve fiber bundles to travel more slowly than light polarized perpendicular to the bundles. The delay experienced by the slower component is called retardance. A multispectral imaging micropolarimeter was used in transmission mode to detect the retardance of the RNFL (Fig. 1). The device has been described in detail previously.[16] Briefly, light from a tungsten-halogen lamp followed by an interference filter (10-nm full width at half maximum) provided monochromatic illumination to an integrating sphere (IS). Lens $L_1$ collimated the beam incident onto a linear polarizer (P). Use of an IS assured that the output intensity of P did not vary as P rotated. Lens $L_2$ focused the exit aperture of IS onto a specimen in a chamber with flat entrance and exit windows. The retinal specimen was mounted with the RNFL on the side facing the exit window. The retina was imaged by lens $L_3$ onto a cooled charge-coupled device (CCD) that provided a pixel size of approximately 3 $\mu$m in an aqueous medium. The response of each pixel was black-level corrected to compensate for the dark current and bias level of the CCD, to produce the measured transmission intensity. To quantify the retardance of the specimen, a liquid crystal retarder (C′) followed by a linear analyzer (A) were located in the detection arm. The retardance of C′ ($\delta_{C'}$) could be varied from 0° to 360°, and the fast axis of C′ could be set to 0°, ±22.5°, and 45°. P and A were Glan-Thompson and Glan-Taylor polarizing prisms, respectively; P could be rotated 360°, and A was fixed at 45°.

## Assessment of the Birefringence of the Retinal Nerve Fiber Bundles

RNFL retardance can be determined with a PC′A polarimeter by measuring the Stokes vectors of the light from the tissue. Usually, eight images are required (see detail in Ref. 16). This method was not suitable for these experiments, because the rapid retardance change during colchicine treatment can distort measurements made from eight sequential images. The birefringence of nerve fiber bundles can be observed in single images, however, when the polarization state exiting the tissue is nearly extinguished by C′A. In the experiments reported herein, the polarization axes of P and A were both set to 45°, and C′ was configured as a half-wave retarder ($\delta_{C'} \approx 180°$) with its fast axis fixed at 0°. With this setting, C′ rotated the plane of the polarization state from P until it was perpendicular to the axis of A, extinguishing the beam to provide a dark field when samples were absent. To observe the retardance of birefringent nerve fiber bundles in this configuration, the bundles were oriented approximately vertically (90° in the polarimeter coordinate system). Contrast between birefringent nerve fiber bundles and the surrounding retina served as a surrogate for retardance. Validity of this alternative was demonstrated by a numerical simulation, as follows.

As shown in the inset of Figure 2A, the retina was simulated as two linear retarders, one for background tissue underlying the RNFL ($R_1$) and the other for nerve fiber bundles only ($R_2$). To take the imperfect

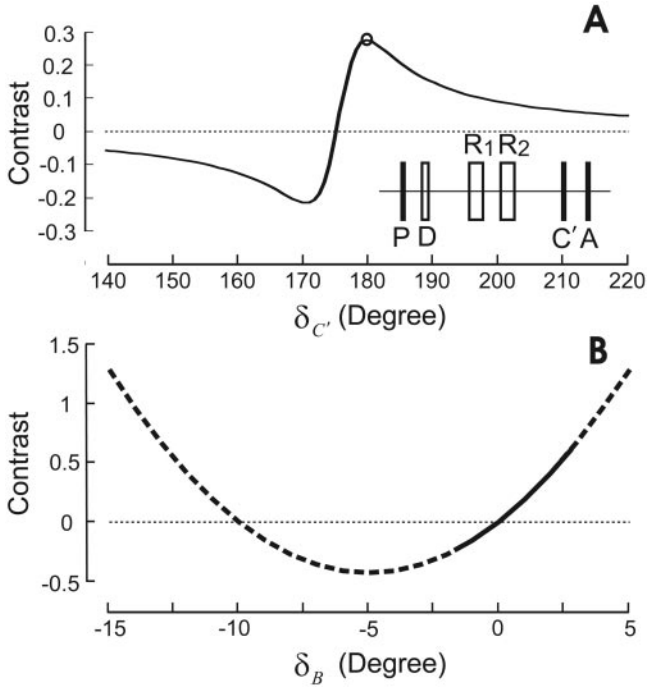


**FIGURE 2.** Numerical simulation of bundle contrast in a PC′A system. P and A were fixed at 45°, and the fast axis of C′ was at 0°. The system had approximately 0.5% depolarization (*D*). The simulated bundle ($R_2$) was oriented at 90° with a retardance of 2 nm, and the background ($R_1$) had a 7-nm retardance with the fast axis at 0°. (**A**) Bundle contrast depended on the retardance of C′ ($\delta_{C'}$). (**B**) With C′ set for the best contrast (*circle* in **A**), bundle contrast varied monotonically with its retardance $\delta_B$ (*solid portion* of the curve).

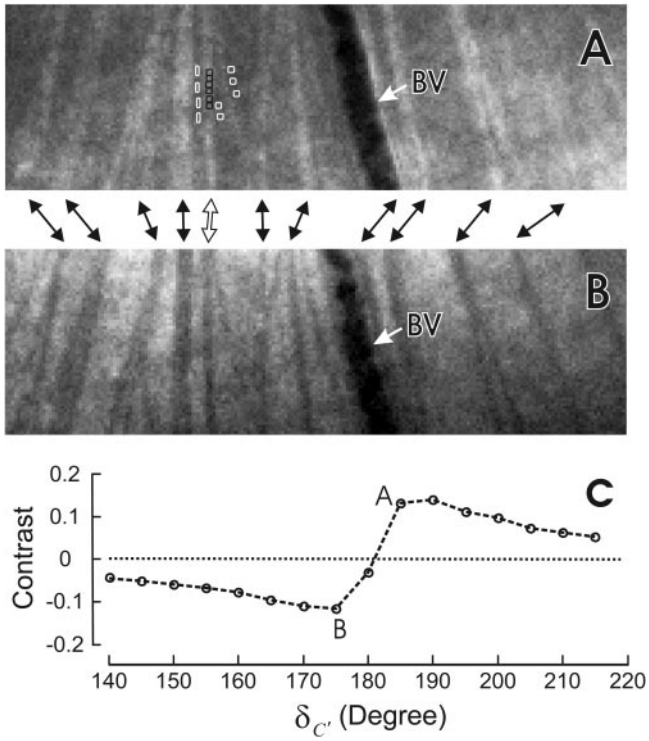


**FIGURE 3.** Isolated rat retina viewed with the polarimeter set near extinction. Retinal nerve fiber bundles (*black arrows*) appeared as bright (**A**) or dark (**B**) bands depending on $\delta_{C'}$. (**A**) $\delta_{C'} = 185°$; (**B**) $\delta_{C'} = 175°$). (**C**) Bundle contrast calculated from the indicated areas on and around the bundle marked with the *open arrow*; $\bar{B}$ varied with $\delta_{C'}$ when the axes of P, C′, and A were fixed. Blood vessels (BV) containing red blood cells appear dark due to strong absorption by hemoglobin at 500 nm. Image size: 800 $\mu$m wide × 240 $\mu$m high.

extinction of the PC′A system into account, we added a weak depolarizer (D) after P. The transmission intensity of the simulated retina was calculated by Mueller calculus.[28,29] Bundle contrast was defined as $B = (R_b - R_g)/R_g$, where $R_b$ was the intensity of a light beam transmitted through a bundle and its background and $R_g$ was the intensity of a light beam transmitted through background only. Parameters used in the simulation were based on retardance measurements of bundles and gaps in a subset of experiments. The simulation showed that $B$ strongly depended on $\delta_{C'}$ (Fig. 2A). To achieve the most sensitive measurement of $B$, $\delta_{C'}$ for the highest $B$ was used. For weak tissue birefringence, $B$ is approximately a parabolic function of bundle retardance $\delta_B$. Due to depolarization, variation of $B$ with $\delta_B$ lies on a monotonic portion of the curve that is approximately linear for small changes in $\delta_B$ (solid curve in Fig. 2B).

In experiments, test images were taken at different $\delta_{C'}$ near 180° until nerve fiber bundles were displayed as bright stripes with best contrast at each wavelength to be tested. Images at these $\delta_{C'}$ were then collected two to three times per minute at 500 nm and every 10 to 20 minutes at 440, 600, 700, and 780 nm throughout an experiment. To ensure that images with best bundle contrast were recorded, we also obtained images at $\delta_{C'} \pm 5°$.

To compare measurements of the same bundles over time, an entire set of images was registered by horizontal and vertical translations. Approximately 10 rectangular measurement areas of 4 to 6 pixels each were chosen both on bundles and on nearby gaps between bundles, and the measured intensities of the pixels in each area were averaged. (Examples of bundle and gap areas are shown in Figs. 3A and 5A.) Only bundles that were oriented near vertical and had approximately uniform surrounding gaps were chosen for analysis. To evaluate changes in birefringence, the contrast of each bundle area was calculated as $B_{ij} = (R_{bi} - R_{gj})/R_{gj}$ ($i, j = 1, 2, \ldots$), where $R_{bi}$ and $R_{gj}$ were the average intensities of the $i$th bundle and $j$th gap areas, respectively. Note that bundle intensity $R_b$ includes contributions of nerve fiber bundles and the underlying retina.[16] Average bundle contrast $\bar{B}$ and the SEM were calculated from all $B_{ij}$ ($i \times j \approx 100$). Data analysis was implemented in MatLab (The MathWorks, Inc., Natick, MA).

## RESULTS

Although the isolated retina was transparent, nerve fiber bundles became visible when viewed by the PC′A polarimeter with $\delta_{C'}$ set to nearly extinguish the polarization state of the beam from the tissue. In agreement with the numerical simulation of the system (Fig. 2A), bundle contrast strongly depended on $\delta_{C'}$ (Fig. 3). Figures 3A and 3B demonstrate that nerve fiber bundles could appear as either bright or dark stripes with different values of $\delta_{C'}$. Figure 3C shows the $\delta_{C'}$ dependence of $\bar{B}$ for one bundle. In the experiments described herein, $\delta_{C'}$ was set to give bright bundles with the best contrast, so that $\bar{B}$ would behave as in Figure 2B. Thus, $\bar{B}$ acted as a surrogate for bundle retardance. A change of $\bar{B}$ indicated a change of retardance and $\bar{B} = 0$ indicated zero bundle retardance (Fig. 2B).

The stability of the preparation was demonstrated by control experiments in which the perfusion solution was switched to an identical baseline solution. Figure 4A shows time courses of bundle contrast in two of these control experiments. To display more clearly temporal change of $\bar{B}$, each bundle in Figure 4A and four more bundles of another retina were normalized by the average of the values in the 10 minutes just before the solutions were switched. The normalized curves were then averaged. Figure 4B shows that $\bar{B}$ was stable throughout the 2 hours of measurement and did not change with the switch of solutions.

In contrast with control experiments, $\bar{B}$ began to decrease immediately after a switch to colchicine solution and was close to zero in approximately 30 minutes. Figure 5 shows an exam-

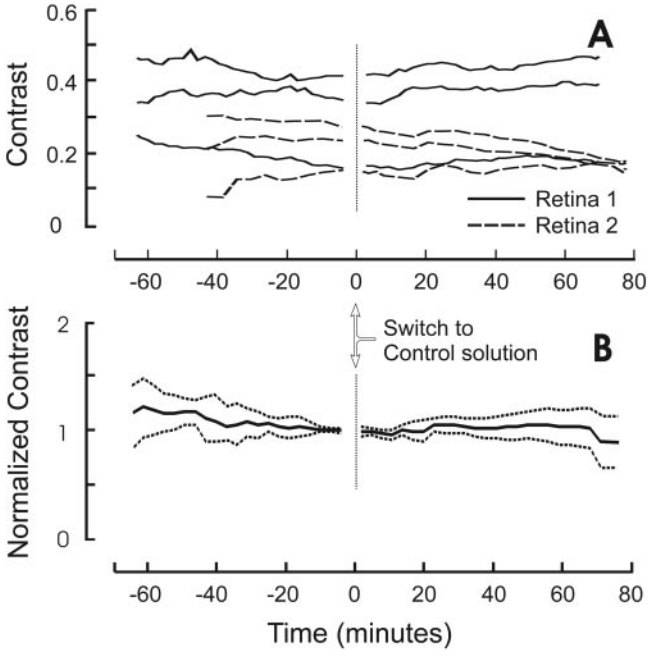


**FIGURE 4.** Control experiments demonstrated the stability of bundle contrast. The perfusate was switched at time 0. (**A**) Time course of $\bar{B}$ for six bundles in two retinas. (**B**) The mean of the normalized $\bar{B}$ (*solid line*) of 10 bundles in three retinas and one SD above and below the mean (*dashed lines*). The normalization level for each area was its average $\bar{B}$ over the 10 minutes before the solution switch.

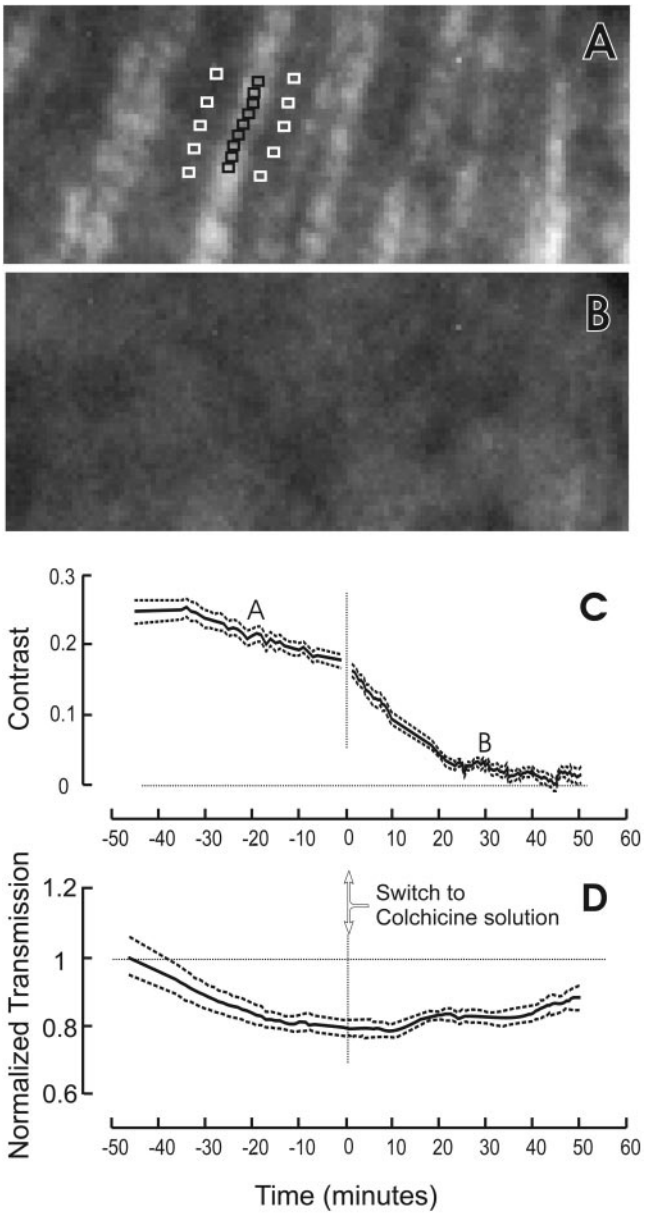


**FIGURE 5.** Colchicine caused $\bar{B}$ to decline. (**A**) Image of nerve fiber bundles 20 minutes before the solution was switched. Bundles appeared as bright stripes. *Black* and *white boxes*: bundle and gap areas, respectively, for one bundle. (**B**) Image of the same retinal region as in (**A**) after 30 minutes of colchicine treatment. Bundles are unobservable. The two images are displayed with the same range of contrast; image size: 480 $\mu$m wide $\times$ 200 $\mu$m high. (**C**) Time course of the $\bar{B}$ (*solid line*) of bundle areas marked in (**A**); *dashed lines*: one SE above and below the mean. The perfusate was switched at time 0. (**D**) *Solid line*: time course of the mean transmission intensity of gap areas normalized to the measurements obtained in the first 2 minutes; *dashed lines*: one SD above and below the mean.

ple of these experiments. Nerve fiber bundles that were bright during the baseline measurements (Fig. 5A) became invisible after 30 minutes of colchicine solution (Fig. 5B). Figure 5C shows the temporal change of $\bar{B}$ for the bundle marked in Figure 5A. $\bar{B}$ was high before the solution switch, decreased rapidly in the first 25 minutes after the switch, and then remained near zero for the rest of the measurements. Although the transmission of the retina usually declined approximately 30% in the first 30 to 40 minutes after placement in the chamber (Fig. 5D), colchicine treatment had no appreciable effect on the appearance of the background.

The effect of colchicine on the retinal background was also evaluated in some experiments by using the polarimeter to measure the Stokes vectors of gap areas. These measurements indicated that the retina exhibited weak retardance (5–9 nm in four retinas). The background retardance did not change very much in 2 hours of measurements and with colchicine treatment.

Figure 6 summarizes the effect of colchicine treatment on $\bar{B}$ for 15 nerve fiber bundles in five retinas (three bundles in each retina). The initial $\bar{B}$ of individual bundles was different across and among retinas. For all bundles, however, $\bar{B}$ dropped after the switch to colchicine solution and for most bundles was close to zero after 30 minutes. To compare with control experiments, Figure 6B shows the normalized and averaged result calculated as described for the control experiments.

Statistical analysis was performed to test whether the final $\bar{B}$ was different from zero. To reduce the variation of a single measurement of $B_{ij}$, the $B_{ij}$ measured for each bundle area over the last 2 minutes of an experiment were averaged. A *t*-test of the averaged $B_{ij}$ showed that $\bar{B}$ was not significantly different from zero ($P > 0.3$) for bundles with at least 70 minutes of colchicine treatment (12 bundles in four retinas), but two of three bundles in one retina with only 50 minutes of colchicine treatment showed $\bar{B} = 0.03$, which was significantly different from zero ($P < 0.01$).

The effect of colchicine on the birefringence of the RNFL was also studied at multiple wavelengths in three of the five retinas shown in Figure 6. Figure 7 illustrates the time courses of $\bar{B}$ at wavelengths of 440, 600, 700, and 780 nm for one of these retinas. For each wavelength, images were taken at the $\delta_{C'}$ for which bundles had best contrast. Bundle contrast was similar for all wavelengths and was stable during baseline

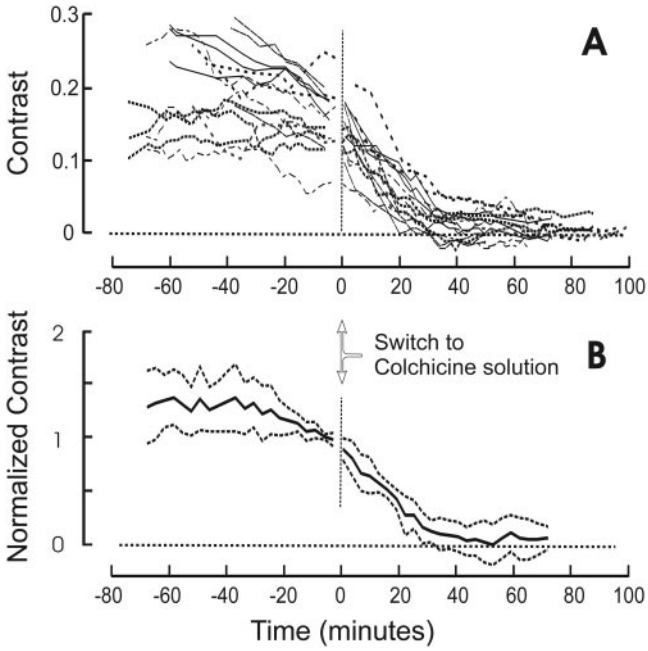


**FIGURE 6.** Temporal change of bundle contrast in colchicine experiments. (**A**) Time course of $\bar{B}$ for 15 bundles in 5 retinas. $\bar{B}$ was high during baseline measurements, declined after the solution was switched to colchicine, and was close to 0 after approximately 30 minutes of treatment; (**B**) normalized and averaged $\bar{B}$ displayed as in Figure 3B. Curves stop at 70 minutes because only a few bundles were observed longer than that.

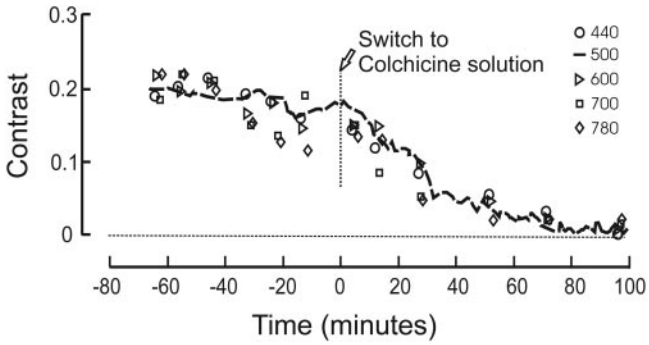


**FIGURE 7.** Temporal change of bundle contrast at different wavelengths in one colchicine experiment. Images were taken every 20 seconds at 500 nm and about every 10 minutes at other wavelengths. $\bar{B}$ was high before the solution switch but declined to near 0 after colchicine treatment at all measured wavelengths.

measurements. After the switch to colchicine solution, nerve fiber bundles faded and became unobservable in approximately 30 minutes at all measured wavelengths. Similar results were found in all nine bundles studied. A *t*-test of the last $B_{ij}$ measured showed that $\bar{B}$ at all measured wavelengths was also not significantly different from zero ($P > 0.5$) for the nine bundles.

## DISCUSSION

Birefringence is an optical property of materials that arises from the interaction of light with oriented molecular and structural components. Many studies have shown that the RNFL exhibits birefringence.[2,8,16,30] A generally accepted assumption is that the RNFL is form birefringent—that is, birefringence is due to an array of thin cylindrical structures in a medium of different refractive index. Candidate structures in the RNFL include MTs, neurofilaments, and axonal membranes. In the present study, colchicine was used to depolymerize MTs in isolated rat retinas, to evaluate the contribution of MTs to RNFL birefringence.

Control retinas perfused with warm, oxygenated physiologic solution demonstrated that RNFL birefringence changed slowly for at least 2 hours. In contrast, colchicine treatment caused RNFL birefringence to decrease rapidly. Nerve fiber bundles disappeared from polarimetry images after approximately 30 minutes of treatment (Fig. 5B) and, even with averaging, were undetectable in all retinas after 70 minutes. Polarimetry showed no major effect of colchicine treatment on retinal tissue in gaps between nerve fiber bundles, and the observed decline in bundle contrast is assumed to be specific to ganglion cell axons, where colchicine is expected to reduce the density of axonal MTs.[24,27] These results imply that MTs contribute significantly to RNFL birefringence.

Birefringence of MTs includes form birefringence, due to the parallel orientation of MTs within axons, and intrinsic birefringence, due to anisotropic macromolecular constituents of individual MTs.[9–11] When the volume fraction of MTs is small, the contributions of intrinsic and form birefringence are both proportional to MT density and are additive.[10,11,14] For the mitotic spindle in an aqueous medium, intrinsic birefringence of MTs is about one tenth as large as form birefringence,[9] implying that form birefringence of MTs is the major mechanism for RNFL birefringence.

A previous study showed that RNFL birefringence varies little across visible and near-infrared wavelengths.[16] The findings in this study that the time course of birefringence decline was similar from 440 to 780 nm (Fig. 7) and that final birefringence of bundles was not different from zero at all tested wavelengths support the idea that MTs are the only structures involved.

The numerical simulation (Fig. 2B) indicates that negative bundle contrast would be observed if there were birefringence components with the slow axis perpendicular to MTs. Bundle contrast of all studied bundles, however, did not decline to noticeable negative values after colchicine treatment. This result suggests that there are no apparent birefringent structures with the slow axis perpendicular to bundles contributing to the RNFL birefringence.

The contribution of other, weaker birefringence mechanisms might be masked by the spatial variability of the intensities from bundle and gap areas that were used to calculate bundle contrast. A maximum value for this contribution can be estimated from the 95% confidence interval on the contrast after it had declined to zero. In 12 bundles of four retinas with at least 70 minutes of colchicine treatment, the 95% confidence interval (two-tailed unpaired *t*-test) ranged from $\pm 0.014$ to $\pm 0.042$. Numerical simulation showed that this contrast corresponds to 9% to 23% (mean = 15%) of the baseline birefringence. Thus, we conclude that in the rat retina mechanisms other than MTs contribute less than 15% to RNFL birefringence.

Electron microscopy (EM) of RNFL in toad retina shows neurofilament density to be higher than MT density, leading to a calculated form birefringence for neurofilaments that is about one third that for MTs, a value that would have been detected in these experiments.[14] This may represent a species difference in neurofilament density or a gap in our understanding of neurofilament properties. For example, no information is available on the intrinsic birefringence of neurofilaments. Quantitative EM is needed to pursue this question.

The results of this study strongly suggest that the dominant source of RNFL birefringence in rat retina is the array of approximately parallel MTs in ganglion cell axons. Ganglion cell axons in both rat and human retinas are unmyelinated, and substantial qualitative differences in optical properties are not expected. The same conclusion, therefore, probably applies to the human RNFL.

These results support the idea that SLP measurements of the RNFL directly indicate the number of MTs intersected by the measuring beam. The reasoning is as follows. In a birefringent material, light polarized in one direction travels more slowly than light polarized in the perpendicular direction. The delay experienced by the slower component is called retardance ($R$) and, for a homogenous material, is proportional to thickness ($T$)—that is $R = \Delta n \times T$, where $\Delta n$ is the birefringence. For an MT array with a small-volume fraction, $\Delta n$ is proportional to MT density.[11,14] SLP measurements, although often expressed as RNFL thickness, actually represent the retardance caused by RNFL birefringence.[2] For beam width $W$ the number of MTs intersected is $N = W \times T \times$ (MT density). Because $\Delta n \propto$ (MT density), it then follows that $R \propto N$. Careful anatomic studies are needed to verify this idea.

Clinical studies have correlated the decrease of RNFL retardance to glaucomatous damage,[4–6] and this study suggests that the damage includes a decrease in the number of axonal MTs. MTs are expected to disappear when axons die, but for early diagnosis and management of glaucoma, it is of great interest to know whether MT density changes before axons die. This knowledge may lie in measurements of $\Delta n$ for the RNFL, either directly with polarization-sensitive optical coherence tomography (OCT)[7,30] or by combining SLP measurements of $R$ with OCT measurements of $T$ and calculating $\Delta n = R/T$.[8] Normal human RNFL can show a two-fold variation in $\Delta n$ on a path around the optic nerve head,[7,8] a variation that may reflect the known structural differences among nerve fiber bundles.[31] The

dependence of $\Delta n$ on axonal structure (MT density) offers hope for the detection of early subcellular changes in glaucoma.

## *References*


1. Pollock SC, Miller NR. The retinal nerve fiber layer. *Int Ophthalmol Clin*. 1986;26:201–221.
2. Dreher AW, Reiter K, Weinreb RN. Spatially resolved birefringence of the retinal nerve-fiber layer assessed with a retinal laser ellipsometer. *Appl Opt*. 1992;31:3730–3735.
3. Zhou Q, Weinreb RN. Individualized compensation of anterior segment birefringence during scanning laser polarimetry. *Invest Ophthalmol Vis Sci*. 2002;43:2221–2228.
4. Weinreb RN, Bowd C, Zangwill LM. Glaucoma detection using scanning laser polarimetry with variable corneal polarization compensation. *Arch Ophthalmol*. 2003;121:218–224.
5. Bagga H, Greenfield DS, Feuer W, Knighton RW. Scanning laser polarimetry with variable corneal compensation and optical coherence tomography in normal and glaucomatous eyes. *Am J Ophthalmol*. 2003;135:521–529.
6. Mohammadi K, Bowd C, Weinreb RN, Medeiros FA, Sample PA, Zangwill LM. Retinal nerve fiber layer thickness measurements with scanning laser polarimetry predict glaucomatous visual field loss. *Am J Ophthalmol*. 2004;138:592–601.
7. Cense B, Chen TC, Park BH, Pierce MC, de Boer JF. Thickness and birefringence of healthy retinal nerve fiber layer tissue measured with polarization sensitive optical coherence tomography. *Invest Ophthalmol Vis Sci*. 2004;45:2606–2612.
8. Huang X-R, Bagga H, Greenfield DS, Knighton RW. Variation of peripapillary retinal nerve fiber layer birefringence in normal human subjects. *Invest Ophthalmol Vis Sci*. 2004;45:3073–3080.
9. Sato H, Ellis GW, Inoue S. Microtubular origin of mitotic spindle form birefringence. *J Cell Biol*. 1975;67:501–517.
10. Bennett HS. The microscopical investigation of biological materials with polarized light. In: McClung CE, ed. *Handbook of Microscopical Technique.* New York: Hafner; 1961:603–609.
11. Oldenbourg R, Salmon ED, Tran PT. Birefringence of single and bundled microtubules. *Biophys J*. 1998;74:645–654.
12. Born M, Wolf E. *Principles of Optics: Electromagnetic Theory of Propagation, Interference, and Diffraction of Light.* Cambridge, UK: Cambridge University Press; 1999.
13. Hogan MJ, Alvarado JA, Weddell JE. *Histology of the Human Eye.* Philadelphia, PA: WB Saunders; 1971.
14. Zhou Q, Knighton RW. Light scattering and form birefringence of parallel cylindrical arrays that represent cellular organelles of the retinal nerve fiber layer. *Appl Opt*. 1997;36:2273–2285.
15. Hemenger RP. Birefringence of a medium of tenuous parallel cylinders. *Appl Opt*. 1989;28:4030–4034.
16. Huang X-R, Knighton RW. Linear birefringence of the retinal nerve fiber layer measured in vitro with a multispectral imaging micropolarimeter. *J Biomed Opt*. 2002;7:199–204.
17. Mitchison JM. A polarized light analysis of the human red cell ghost. *J Exp Biol*. 1953;30:397–432.
18. Inoue S. The effect of colchicine on the microscopic and submicroscopic structure of the mitotic spindle. *Exp Cell Res.* 1952; 2(suppl):305–318.
19. Rome-Talbot D, Andre D, Chalazonitis N. Hypothermic decrease in microtubule density and birefringence in unmyelinated axons. *J Neurobiology*. 1978;9:247–254.
20. Darnell J, Lodish H, Baltimore D. *Molecular Cell Biology.* New York: Scientific American Books; 1990:820–822.
21. Eigsti OJ, Dustin PJ. *Colchicine*: *In Agriculture, Medicine, Biology and Chemistry.* Ames, IA: The Iowa State College Press; 1955.
22. Weisenberg RC, Borisy GG, Taylor EW. The colchicine-binding protein of mammalian brain and its relation to microtubules. *Biochemistry*. 1968;7:4466–4478.
23. Skoufias DA, Wilson L. Mechanism of inhibition of microtubule polymerization by colchicine: inhibitory potencies of unliganded colchicine and tubulin-colchicine complexes. *Biochemistry*. 1992; 31:738–746.
24. Donoso JA. Microtubule stability along mammalian peripheral nerves. *J Neurobiol*. 1986;17:383–403.
25. Huang X-R, Knighton RW. Diattenuation and polarization preservation of retinal nerve fiber layer. *Appl Opt*. 2003;42:5737–5743.
26. Knighton RW, Huang X-R. Visible and near-infrared imaging of the nerve fiber layer of the isolated rat retina. *J Glaucoma*. 1999;8: 31–37.
27. Knighton RW, Huang X-R, Zhou Q. Microtubule contribution to the reflectance of the retinal nerve fiber layer. *Invest Ophthalmol Vis Sci*. 1998;39:189–193.
28. Azzam RMA, Bashara NM. *Ellipsometry and Polarized Light.* New York: North-Holland; 1989.
29. Chipman RA. Polarimetry. In: *Handbook of Optics.* Bass M, van Stryland EW, Williams DR, Wolfe WL, eds. New York: McGraw-Hill, Inc.; 1995:22.21–22.37.
30. Cense B, Chen TC, Hyle Park B, Pierce MC, de Boer JF. *In vivo* birefringence and thickness measurements of the human retinal nerve fiber layer using polarization-sensitive optical coherence tomography. *J Biomed Opt*. 2004;9:121–125.
31. Ogden TE. Nerve fiber layer of the primate retina: morphometric analysis. *Invest Ophthalmol Vis Sci*. 1984;25:19–29.